

Hook-Based Aerial Payload Grasping from a Moving Platform

Péter Antal¹, Tamás Péni¹, and Roland Tóth^{1,2}

Abstract—This paper investigates payload grasping from a moving platform using a hook-equipped aerial manipulator. First, a computationally efficient trajectory optimization based on complementarity constraints is proposed to determine the optimal grasping time. To enable application in complex, dynamically changing environments, the future motion of the payload is predicted using physics simulator-based models. The success of payload grasping under model uncertainties and external disturbances is formally verified through a robustness analysis method based on integral quadratic constraints. The proposed algorithms are evaluated in a high-fidelity physical simulator, and in real flight experiments using a custom-designed aerial manipulator platform.

SUPPLEMENTARY MATERIAL

A video summarizing the paper and showcasing the experiments is available at <https://youtu.be/PNdkaovkc5I>.

I. INTRODUCTION

There is a growing interest to perform intricate tasks with unmanned aerial vehicles (UAVs) that require robotic manipulation and direct physical interaction with the environment [1]–[3]. Payload transportation has been extensively studied in aerial manipulation, but many challenges still need to be addressed. A key challenge is to fully automate the procedure, requiring both the grasping and placement of the payload to be performed without human intervention. Furthermore, in industrial settings, the transportation has to meet strict scheduling requirements, such as being completed within a specific time window or in minimal time [4].

Payload grasping from a moving platform is particularly challenging as it requires precise coordination of the manipulator with the trajectory of the payload. The problem has been first considered in [5], where the authors proposed a time-optimal planning method based on motion primitives. The applicability of the method is limited by the assumption that the trajectory of the moving platform is exactly known, and the performance of the approach has been only analyzed in simulations. In [6], a 7 DoF robotic arm is attached to a quadcopter to grasp a moving payload. Although the experimental results show successful execution, the solution relies on baseline methods, such as PID control, therefore versatility is limited and optimality cannot be ensured. The current state-of-the-art work [7] presents a time-optimal trajectory planning method for a quadcopter equipped with a 1 DoF robotic

This research was supported by the European Union within the framework of the National Laboratory for Autonomous Systems (RRF-2.3.1-21-2022-00002).

¹The authors are with the Systems and Control Lab, HUN-REN Institute for Computer Science and Control, Budapest, Hungary (email: antalpeter@sztaki.hun-ren.hu, peni@sztaki.hun-ren.hu, r.toth@tue.nl).

²Roland Tóth is also affiliated with the Control Systems Group of the Eindhoven University of Technology, The Netherlands.

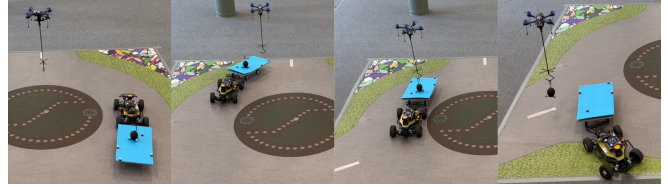


Fig. 1. Payload grasping from an UGV with a hook-based manipulator.

manipulator and an electromagnetic gripper. The algorithm is able to automatically find optimal handover opportunities by employing complementarity constraints. However, there is still room for improvement in certain areas, namely (i) the weight and power consumption of the manipulator reduce energy efficiency, (ii) the payload mass is not considered in the dynamic model used for planning that can degrade the performance of trajectory design, (iii) the future trajectory of the payload is assumed to be exactly known during the entire the maneuver, which is difficult to guarantee in many real-world scenarios, (iv) the trajectory optimization is complex and highly nonlinear, resulting in a computation time exceeding 10 s that makes it difficult to use when real-time replanning is needed, and (v) model uncertainties and external disturbances are not considered in the design, therefore robustness w.r.t. these effects is unknown.

In this work, we investigate hook-based aerial grasping from a moving platform, illustrated in Fig. 1. The hook is attached to a rigid rod, connected to the drone via an unactuated 2 DoF joint. Hook-based transportation has several advantages over using flexible cables [8]–[11] or robotic extensions [6], [7], [12] by combining energy efficiency, good maneuverability, and autonomous grasping ability [13].

Using the hook-based manipulator, we intend to grasp a payload (with a hook attached on top) that is located on a moving unmanned ground vehicle (UGV). To address the limitations of previous works, first, instead of assuming perfect knowledge of the future motion of the payload, we use digital twin models for prediction based on the current position and velocity of the vehicle, and the task-specific reference path. Then, we explicitly consider the payload mass in trajectory planning and formulate the optimization such that it can be solved by sequential quadratic programming with real-time iterations (SQP-RTI) to enhance computational efficiency. Finally, we apply integral quadratic constraints (IQCs) for robustness analysis of the closed-loop system governed by an LTV-LQR controller. As a result, we are able to verify successful grasping under model uncertainties and external disturbances. Our contributions are as follows:

- C1 We propose a trajectory optimization method by complementarity constraints to automatically find the optimal grasping time instant within a pre-specified time window. The low computational cost of the SQP-RTI optimization and the digital twin-based payload motion prediction enable rapid replanning of the trajectory in response to environmental changes.
- C2 We propose a robustness analysis method by integral quadratic constraints to theoretically guarantee successful grasping under uncertainties and disturbances.
- C3 To demonstrate the performance of the methods, first, we conduct simulations in which the UGV navigates on an unknown, continuously changing rough terrain. Then, we perform real flight experiments.

II. MODELLING

Similar to the models commonly used to design controllers for cable-based transportation [14], [15], we model the quadcopter and the payload as a rigid body and a point mass, respectively. Moreover, we neglect the mass of the rigid bar, and lump together the mass of the hook and the payload. Unlike the models used in [14], [15], we take into account viscous friction in the joint connecting the hook to the drone.

Three main frames are used to express the system configuration: the inertial frame (\mathcal{F}^i), the quadcopter body frame (\mathcal{F}^b), and the payload frame (\mathcal{F}^l), as it is illustrated in Fig. 2. We derive the model using the following state representation:

$$\xi = [r^\top \quad \dot{r}^\top \quad \lambda^\top \quad \omega^\top \quad \alpha \quad \beta \quad \dot{\alpha} \quad \dot{\beta}]^\top \in \mathbb{R}^{16}, \quad (1)$$

where $r(t) \in \mathbb{R}^3$ is the drone position in \mathcal{F}^i , $\lambda = [\phi \ \theta \ \psi]^\top$, $\lambda(t) \in \mathbb{R}^3$ contains the RPY (roll ϕ , pitch θ , yaw ψ) angles, $\omega(t) \in \mathbb{R}^3$ is the angular velocity, and $\alpha(t), \beta(t) \in \mathbb{R}$ represent the rotation of \mathcal{F}^l w.r.t \mathcal{F}^i . The payload position and derivatives are expressed from the states, as follows:

$$r_L = r + Lq, \quad \dot{r}_L = \dot{r} + L\dot{q}, \quad \ddot{r}_L = \ddot{r} + L\ddot{q}, \quad (2a)$$

$$q = [-\cos \alpha \sin \beta \quad \sin \alpha \quad -\cos \alpha \cos \beta]^\top, \quad (2b)$$

where $q(t) \in \mathbb{R}^3$ is the unit vector pointing from the quadcopter CoM to the payload CoM.

To derive the dynamic model, we take the equations of motion from [16] corresponding to the payload suspension:

$$\begin{aligned} m\ddot{r} &= FRe_3 - mge_3 + Tq, \\ m_L\ddot{r}_L &= -Tq - m_Lge_3, \quad J\dot{\omega} + \omega \times J\omega = \tau, \end{aligned} \quad (3)$$

where m, m_L are the mass of the quadcopter and the payload (with the hook), $e_3 = [0 \ 0 \ 1]^\top$, $T(t) \in \mathbb{R}$ is the force on the rigid bar, $R(t) \in \text{SO}(3)$ is the rotation matrix on the special orthogonal group, $J = \text{diag}(J_x, J_y, J_z)$ is the inertia matrix of the quadcopter, assumed to be diagonal, and $F(t) \in \mathbb{R}, \tau \in \mathbb{R}^3$ are force and torque inputs generated by the propellers. Based on [14], the dynamics of q are described, as follows:

$$\ddot{q} = (mL)^{-1} (q \times (q \times FRe_3)) - (\dot{q}^\top \dot{q})q. \quad (4)$$

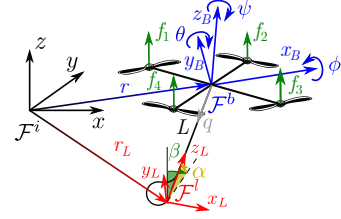


Fig. 2. Quadrotor-hook model with the three main coordinate frames.

The position dynamics are formulated by combining (2)-(4):

$$\begin{aligned} \ddot{r} &= f_r(q, \dot{q}, R, F) = (m + m_L)^{-1} FRe_3 - ge_3 \\ &\quad - \frac{m_L L}{m + m_L} \left(\frac{1}{mL} (q \times (q \times FRe_3)) - (\dot{q}^\top \dot{q})q \right). \end{aligned} \quad (5)$$

In the next step, we formulate the equations of the two revolute joints by expressing α and β from (2b), differentiating it two times, and substituting (4) into \ddot{q} , as follows: $[\ddot{\alpha} \ \ddot{\beta}]^\top = f_L(q, \dot{q}, R, F)$. Due to the use of inverse trigonometric functions, f_L is singular if the orientation of the rod becomes horizontal. However, during payload grasping and transportation, we avoid such large swing angles.

We complete the model by putting together the above equations and adding a viscous friction term to the dynamics of the revolute joints, as follows:

$$\dot{\xi} = f(\xi, u) = \begin{bmatrix} \dot{r} \\ f_r(q, \dot{q}, R, F) \\ Q^{-1}\omega \\ J^{-1}(\tau - \omega \times J\omega) \\ [\dot{\alpha} \ \dot{\beta}]^\top \\ f_L(q, \dot{q}, R, F) - b[\dot{\alpha} \ \dot{\beta}]^\top \end{bmatrix}, \quad (6)$$

where $Q(t) \in \mathbb{R}^{3 \times 3}$ is the standard transformation matrix from the derivatives of the Euler angles to the angular velocity [17], and $b \in \mathbb{R}^+$ is the viscous friction coefficient, the numerical value of which is obtained by measuring the logarithmic decrement of the hook oscillations while the quadcopter body is fixed [18].

Although (6) captures the full dynamics of the aerial manipulator, the position and velocity of the payload are not explicitly expressed by the state vector. In trajectory planning, as multiple constraints are required for the payload states, we modify the state vector as follows:

$$\tilde{\xi} = [r_L^\top \quad \dot{r}_L^\top \quad \lambda^\top \quad \omega^\top \quad \alpha \quad \beta \quad \dot{\alpha} \quad \dot{\beta}]^\top \in \mathbb{R}^{16}. \quad (7)$$

Then, if (4), (5) are substituted into (2a), we can arrive at

$$\ddot{r}_L = f_{r_L}(q, \dot{q}, R, F) = \frac{1}{m + m_L} (q^\top FRe_3 - mL\dot{q}^\top \dot{q})q - ge_3.$$

Finally, the complete equations of motion are as follows:

$$\dot{\tilde{\xi}} = \tilde{f}(\tilde{\xi}, u), \quad (8)$$

where \tilde{f} is the same as f in (6), except for replacing \dot{r} by \dot{r}_L and f_r by f_{r_L} .

III. TRAJECTORY PLANNING

A. Payload motion prediction

In prior works, the future trajectory of the moving payload is typically assumed to be exactly known [5]–[7]. In contrast, we only assume that the task-specific reference path of the UGV and the structure of the environment are known a few seconds before grasping. For prediction, we use the digital twin model of the UGV, the manipulator, and the payload, which has been implemented in MuJoCo [19], a high-fidelity physics engine that is able to simulate complex dynamics with collisions and contacts.

A key challenge in digital twin-based prediction is the accurate initialization of the simulation. Although we assume that all states can be measured or computed from the kinematics, imperfect measurements may cause significant variations in the simulated contact forces. To enhance robustness w.r.t. initial conditions, we simulate the UGV dynamics in closed loop with a low-level controller. In simulation experiments, we test this robustness by adding white Gaussian noise to the initial states. Our results, detailed in Section VI, show that the grasping is accomplished in dynamically changing environments that confirms practical effectiveness of the approach. Nonetheless, more advanced algorithms could be employed for initialization, see e.g. [20].

B. Planning concept

Motivated by the strict schedule of industrial processes, we define a time window, within which the quadcopter has to grasp the payload:

$$0 < \underline{T}_g \leq T_g \leq \bar{T}_g < T_f, \quad (9)$$

where the beginning and end of the time window ($\underline{T}_g, \bar{T}_g$), together with the duration (T_f) are fixed in the problem description, and the grasp time (T_g) is a decision variable.

For payload grasping and transportation, we propose a nonlinear optimization-based trajectory planning method. First, as it is illustrated on Fig. 3, we divide the motion to three phases: 1) approach the moving payload; 2) attach the hook; 3) transport the payload above the target location. Phase 1 takes until the beginning of the grasping time window. Meanwhile, the quadcopter has to approach the payload to get ready for grasping. In Phase 2, the aerial manipulator has to grasp the payload by attaching the hook. At the end of the grasping time window, Phase 3 starts, where the goal is to transport the payload above the target location.

To perform successful grasping, the motion of the quadcopter is coordinated with the trajectory of the payload. First, the hook of the quadcopter and the payload are aligned to be perpendicular at the grasping time instant. Second, at that point, a target velocity is prescribed for the hook, defined as the sum of the payload velocity and a relative velocity term that is parallel to the body x axis of the payload. These conditions are formulated as follows:

$$[\psi_r, v_r] = \begin{cases} [\psi_p, (1 + \tau R_z(\bar{\psi}_p))v_p] & \text{if } |\bar{\psi}_p| \leq \frac{\pi}{2} \\ [\psi_p - \vartheta, (1 + \tau R_z(\bar{\psi}_p - \vartheta))v_p] & \text{otherwise} \end{cases} \quad (10)$$

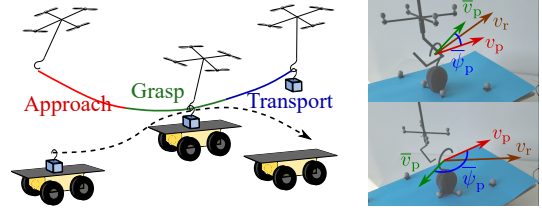


Fig. 3. Left: 3 phases of the motion trajectory, right: grasping conditions.

where $\psi_p \in \mathbb{R}, v_p \in \mathbb{R}^3$ are the yaw angle and velocity of the payload, $\bar{\psi}_p \in \mathbb{R}$ is the angle between the velocity and body x axis of the payload, $\bar{v}_p \in \mathbb{R}^3$ denotes v_p rotated by $\bar{\psi}_p$ around the z axis of the inertial frame, $\psi_r \in \mathbb{R}, v_r \in \mathbb{R}^3$ are the target yaw and velocity of the hook, $\vartheta = \text{sgn}(\bar{\psi}_p)\pi/2$, and R_z denotes the rotation matrix around the z axis of the inertial frame. The user-defined parameter $\tau \in \mathbb{R}^+$ determines the relative velocity of the hook, increasing its value leads to more aggressive grasping. The grasping conditions are illustrated in Fig. 3.

C. Trajectory optimization

Discretization: We formulate the trajectory optimization in discrete time to exploit the benefits of multiple shooting methods [21]. The dynamic model (8) is discretized by 4th order Runge-Kutta method with sampling time $h \in \mathbb{R}^+$ as $\tilde{\xi}_d(k+1) = \tilde{f}_{\text{RK4}}(\tilde{\xi}_d(k), u_d(k))$, where $k \in \mathbb{Z}$ is the discrete time index with $t = kh$, and $\xi_d(k) \in \mathbb{R}^{16}, u_d(k) \in \mathbb{R}^4$ are the states and inputs. The time window parameters are also adjusted to the sampling time as $\underline{N}_g = \lceil \underline{T}_g/h \rceil, \bar{N}_g = \lceil \bar{T}_g/h \rceil, N_f = \lceil T_f/h \rceil$, where $\lceil x \rceil$ denotes the nearest integer to x .

Cost function: For each of the three phases, we introduce different cost terms and constraints, according to the current planning objective. Then, we combine the three phases into one optimization problem. We use quadratic running costs:

$$l_i(k) = \|\tilde{\xi}_d(k) - \tilde{\xi}_r^i(k)\|_{W_Q^i}^2 + \|u_d(k) - u_r^i(k)\|_{W_R^i}^2 \quad (11)$$

for $i = 1, 2, 3$, where $W_Q^i \in \mathbb{R}^{16 \times 16}, W_R^i \in \mathbb{R}^{4 \times 4}$ are positive semidefinite weight matrices and $\tilde{\xi}_r^i, u_r^i$ denote target states and inputs that are explained next for each phase.

The objective of Phase 1 is to approach the moving payload, which we solve by following the trajectory of the ground vehicle with a delay of $T_d \in \mathbb{Z}^+$ time steps. Accordingly, we define the target state as follows:

$$\tilde{\xi}_r^1(k) = [r_p(k - T_d)^\top \quad 0_5 \quad \psi_r(k - T_d) \quad 0_8]^\top, \quad k \in [0, \underline{N}_g]$$

where r_p is the payload position and ψ_r is given by (10).

In Phase 2, the payload needs to be grasped from the moving platform. Consequently, we set the target state based on (10), as follows:

$$\tilde{\xi}_r^2(k) = [r_p(k)^\top \quad v_r(k)^\top \quad 0_2 \quad \psi_r(k) \quad 0_8]^\top, \quad k \in [\underline{N}_g, \bar{N}_g]$$

In Phase 3, the objective is to transport the payload to the user-defined target location $r_{L,f}$ with target yaw ψ_f , therefore we define $\tilde{\xi}_r^3(k) = \tilde{\xi}_{d,f} = [r_{L,f}^\top \quad 0_5 \quad \psi_f \quad 0_8]^\top$ for $k \in [\bar{N}_g, N_f]$.

The input term of the cost function (11) is used to avoid aggressive movements of the quadcopter, therefore we

penalize the applied control effort compared to hovering with $u_r^i = [(m + m_L)g \ 0 \ 0 \ 0]^\top$ for $i = 1, 2, 3$.

Constraints: We bound the states and control inputs of the manipulator, as follows:

$$u_{d,\min} \leq u_d(k) \leq u_{d,\max}, \quad \tilde{\xi}_{d,\min} \leq \tilde{\xi}_d(k) \leq \tilde{\xi}_{d,\max}, \quad (12)$$

where $u_{d,\min}, u_{d,\max}$ represent the actuator limits of the quadcopter, and $\tilde{\xi}_{d,\min}, \tilde{\xi}_{d,\max}$ are specified by the user based on e.g. the available flying space or safety considerations.

To ensure that the hook of the quadcopter and the payload get attached, we employ *complementarity constraints*, similar to [7]. For this, we introduce the index variable $\varepsilon(k) \in \mathbb{R}$ to indicate whether the grasping conditions given by (10) are satisfied. Then, we formulate the following constraints:

$$\begin{aligned} \varepsilon(k)f_{gr}(k) &= 0, \quad \varepsilon(k) \in [0, 1] \\ f_{gr}(k) &= \|r_L(k) - r_P(k)\| + \|\psi(k) - \psi_r(k)\| + \|\dot{r}_L(k) - v_r(k)\|. \end{aligned} \quad (13)$$

To ensure that $\varepsilon(k) > 0$ and $f_{gr}(k) = 0$ at least once in Phase 2, we introduce the cumulative index variable $\kappa(k) \in \mathbb{R}$:

$$\kappa(k+1) = \kappa(k) - \varepsilon(k), \quad \kappa(0) = 1, \quad \kappa(N_f) = 0. \quad (14)$$

Since $\kappa(0) > \kappa(N_f)$, $\varepsilon(k)$ is forced to be nonzero at some point of the trajectory, implying that the grasping conditions are satisfied.¹ In practice, strict complementarity constraints are difficult to handle by numerical solvers [7], therefore we relax (13) by introducing a slack variable ν , as follows:

$$\varepsilon(k)(f_{gr}(k) - \nu(k)) = 0, \quad 0 \leq \nu(k) \leq \nu_{\max}, \quad (15)$$

where $\nu_{\max} \in \mathbb{R}$ is set to a small constant, e.g. 10^{-3} .

Optimal control problem: We formulate trajectory planning as a finite-horizon optimal control problem (OCP) by putting together the cost function and constraints. For this, we incorporate the complementarity variables into the dynamic model, resulting in the augmented states $\bar{\xi}_d = [\tilde{\xi}_d^\top \ \kappa]^\top$, augmented inputs $\bar{u}_d = [u_d^\top \ \varepsilon \ \nu]^\top$, and augmented dynamics $\bar{f}(\bar{\xi}_d, \bar{u}_d) = [f_{RK4}(\tilde{\xi}_d, \bar{u}_d)^\top \ \kappa - \varepsilon]^\top$. Now, (11)-(15) are combined to formulate the OCP:

$$\text{minimize}_{\bar{\xi}_d(k), \bar{u}_d(k), N_g} J = \sum_{k=0}^{N_g-1} l_1(k) + \sum_{k=N_g}^{\bar{N}_g-1} l_2(k) + \sum_{k=N_g}^{N_f-1} l_3(k) \quad (16a)$$

$$\text{subject to } \bar{\xi}_d(0) = \bar{\xi}_{d,0}, \quad \bar{\xi}_d(N_f) = \bar{\xi}_{d,f} \quad (16b)$$

$$\varepsilon(k)(f_{gr}(k) - \nu(k)) = 0 \quad k \in [N_g, \bar{N}_g] \quad (16c)$$

$$\varepsilon(k) = 0 \quad k \notin [N_g, \bar{N}_g] \quad (16d)$$

$$\bar{\xi}_d(k+1) = \bar{f}(\bar{\xi}_d(k), \bar{u}_d(k)) \quad (16e)$$

$$m_L = m_{\text{hook}} + (1 - \kappa)m_{\text{load}} \quad (16f)$$

$$\bar{\xi}_{d,\min} \leq \bar{\xi}_d(k) \leq \bar{\xi}_{d,\max} \quad (16g)$$

$$\bar{u}_{d,\min} \leq \bar{u}_d(k) \leq \bar{u}_{d,\max} \quad (16h)$$

where $\bar{\xi}_{d,0}, \bar{\xi}_{d,f}, \bar{\xi}_{d,\min}, \bar{\xi}_{d,\max}, \bar{u}_{d,\min}, \bar{u}_{d,\max}$ correspond to the boundary conditions given by (13)-(15). Note that (16f)

¹The constraint formulation would allow for $\varepsilon(k) > 0$ at separate time instants, resulting in multiple grasping points. However, we restrict the time window $[T_g, \bar{T}_g]$ such that dynamically feasible trajectories only exist with one grasp point, where $\varepsilon(k) = 1$.

ensures that the mass of the load is added to the mass of the hook automatically after the grasping time instant, without knowing the value of N_g a priori. Hence, we make sure that the effect of the payload on the dynamics is directly considered in the physical model, therefore the optimized trajectory is dynamically feasible (in contrast e.g. to [7]).

To solve Optimization (16), we use the sequential quadratic programming with real-time iterations (SQP-RTI) solver of Acados [22]. Although the dynamics and complementarity constraints are nonlinear, the cost function is quadratic and most constraints are linear. This leads to a computation time of around 0.4 s on a standard laptop, which enables real-time replanning. To replan the trajectory at time step $k = N_{rp}$, we shift the time window by subtracting N_{rp} from N_g, \bar{N}_g, N_f , and solve (16) on a shrunk horizon [23].

IV. TRAJECTORY TRACKING

Due to its generality, low complexity, and computational efficiency, we design a linear time-varying linear-quadratic regulator (LTV-LQR) [24] to follow the optimized reference trajectory. To synthesize the controller, we linearize the equations of motion (6) along the reference trajectory by first-order Taylor expansion: $\xi \approx f(\xi^*, u^*) + A(\xi - \xi^*) + B(u - u^*)$, where $A(t) \in \mathbb{R}^{16 \times 16}, B(t) \in \mathbb{R}^{16 \times 4}$ are the time-varying state and input matrices, respectively. The reference states and inputs $\xi^*(t), u^*(t)$ are obtained by solving Optimization (16), interpolating the discrete-time states and inputs by splines, and applying (2a) to transform between the state representations (7) and (1). By introducing the error state $\eta = \xi - \xi^*$ and input $v = u - u^*$, the linear time-varying error dynamics are written, as follows:

$$\dot{\eta}(t) = A(t)\eta(t) + B(t)v(t). \quad (17)$$

Then, the optimal feedback gain matrix is computed as the solution of a finite-horizon LQ optimization problem:

$$\begin{aligned} &\text{minimize}_v \int_0^{T_f} (\|\eta(t)\|_{\mathcal{W}_Q}^2 + \|v(t)\|_{\mathcal{W}_R}^2) dt + \|\eta(T_f)\|_{\mathcal{W}_F}^2 \\ &\text{subject to } v(t) = -K(t)\eta(t), \end{aligned} \quad (18)$$

where $\mathcal{W}_Q, \mathcal{W}_F \in \mathbb{R}^{16 \times 16}, \mathcal{W}_R \in \mathbb{R}^{4 \times 4}$ are positive semidefinite state and input weight matrices and $K(t) \in \mathbb{R}^{4 \times 16}$ is the time-varying feedback gain matrix.

V. IQC-BASED ROBUSTNESS ANALYSIS

A. Uncertain dynamics

The equations of motion given by (6) describe the nominal dynamics of the aerial manipulator. However, in reality, the exact value of the parameters are hard to determine, and other uncertainties may also be present, e.g. due to unmodeled actuator dynamics or aerodynamics [25]. These uncertainties may deteriorate the precision of the motion which could eventually lead to unsuccessful payload grasping. In this section, we introduce an uncertain model of the system and compute its *robust \mathcal{L}_2 -to-Euclidean gain* [26] to characterize the worst-case hook position error at the grasping time instant. If the worst-case error is smaller than the radius of the hook, then the grasping is guaranteed to be successful.

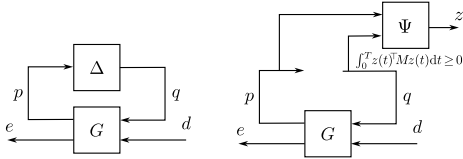


Fig. 4. Left: Interconnection of nominal LTV system G and uncertainty Δ with disturbance input d and performance output e . Right: Extended LTV system with IQC filter Ψ . [26]

We consider the x, y inertia elements and the viscous friction of the joint as uncertain parameters collected to $\tilde{\delta} = [J_x \ J_y \ b]^\top$ with nominal values $\varphi_0 = [J_{x,0} \ J_{y,0} \ b_0]^\top$ and uncertainty range $\bar{\varphi} \in \mathbb{R}^3$ such that $\tilde{\delta} \in [\varphi_0 - \bar{\varphi}, \varphi_0 + \bar{\varphi}]$. We normalize the uncertainties as $\tilde{\delta} = \varphi_0 + \text{diag}(\bar{\varphi})\delta$. Then, we take the closed-loop nominal LTV system G given by (17), (18) and formulate a *linear fractional representation* (LFR) by separating the normalized uncertainties to $\Delta = \text{diag}(\delta_1 I_{n_1}, \delta_2 I_{n_2}, \delta_3 I_{n_3})$, where $n_1 = n_2 = 3, n_3 = 2$ are the dimensions corresponding to the linearizations in $\tilde{\delta}$. For external disturbance, we consider a scalar force $d(t) = \delta F(t)$, $\|d\|_{2,[0,T]} \leq \beta$ added to the thrust control input of the quadrotor, representing unmodeled aerodynamic effects. According to the objective of this analysis, the output of the system $e(t)$ is the position error of the hook. The block diagram of the resulting uncertain system is shown in Fig. 4, and it is described by the finite-time state-space model G_Δ :

$$\begin{aligned} \dot{\eta}(t) &= A_G(t)\eta(t) + B_{G1}(t)q(t) + B_{G2}(t)d(t), \\ p(t) &= C_{G1}(t)\eta(t) + D_{G11}(t)q(t) + D_{G12}(t)d(t), \\ e(t) &= C_{G2}(t)\eta(t) + D_{G21}(t)q(t) + D_{G22}(t)d(t) \end{aligned} \quad (19)$$

for $t \in [0, T]$, where $A_G(t) = A(t) - B(t)K(t)$, $p(t) \in \mathbb{R}^{n_p}$ is the input and $q(t) \in \mathbb{R}^{n_q}$ is the output corresponding to Δ with $n_p = n_q = n_1 + n_2 + n_3$. The finite-horizon \mathcal{L}_2 -to-Euclidean gain of the uncertain LTV system G_Δ is $\|G_\Delta\|_{E,[0,T]} = \sup_{\|d\|_{2,[0,T]} \neq 0} \left\{ \frac{\|e(T)\|}{\|d\|_{2,[0,T]}} \right\}$.

B. Integral quadratic constraints

To compute the robust \mathcal{L}_2 -to-Euclidean gain of the closed-loop system, we employ *integral quadratic constraints* (IQCs) [27]. Let $\Psi \in \mathbb{RH}_\infty^{n_z \times (n_p + n_q)}$ be a stable rational proper transfer function with $z = \Psi(p, q)$ and $M : [0, T] \rightarrow \mathbb{S}^{n_z}$ a piecewise continuous matrix function. The input-output signals $p \in \mathcal{L}_2^{n_p}[0, T]$ and $q = \Delta(p)$ satisfy the time-domain IQC defined by (Ψ, M) if the following holds for all $\Delta : \mathcal{L}_2^{n_p}[0, T] \rightarrow \mathcal{L}_2^{n_q}[0, T]$:

$$\int_0^T z(t)^\top M(t) z(t) dt \geq 0, \quad (20)$$

where p, q are filtered through Ψ with zero initial conditions. Our goal is to represent the uncertain relation by finding $M(t)$ such that (20) is satisfied for any $z(t)$ produced through Δ with the smallest conservatism. As our system contains parametric uncertainty, we search for M with a block diagonal structure $M = \text{diag}(M^1, M^2, M^3)$, where

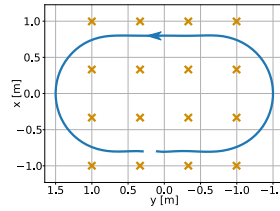


Fig. 5. UGV reference path used for the experiments (blue), and initial drone positions used for robustness analysis (orange).

TABLE I
PHYSICAL PARAMETERS OF THE MANIPULATOR.

m	$6.05 \cdot 10^{-1}$	kg
m_{hook}	$1 \cdot 10^{-2}$	kg
$J_{x,0}$	$1.5 \cdot 10^{-3}$	kg m ²
δJ_x	$3 \cdot 10^{-4}$	kg m ²
$J_{y,0}$	$1.45 \cdot 10^{-3}$	kg m ²
δJ_y	$3 \cdot 10^{-4}$	kg m ²
J_z	$2.66 \cdot 10^{-3}$	kg m ²
L	$4 \cdot 10^{-1}$	m
b_0	$2.9 \cdot 10^{-1}$	rad s
δb	$1 \cdot 10^{-1}$	rad s

each block is parametrized as follows [27], [28]:

$$M^i := \begin{bmatrix} M_{11}^i & M_{12}^i \\ (M_{12}^i)^\top & -M_{11}^i \end{bmatrix} \quad \text{for } i = 1, 2, 3 \quad (21)$$

where $M_{11}^i = (M_{11}^i)^\top \succeq 0$ and $M_{12}^i = -(M_{12}^i)^\top$ are constant real matrices. Inspired by [26], we parametrize Ψ as $\Psi = \text{diag}(\Psi^1, \Psi^2, \Psi^3)$, $\Psi^i = \text{diag}(\psi_{11}^i, \psi_{11}^i)$, $\psi_{11}^i = [1 \ \frac{1}{s+\lambda}]^\top$, $\lambda > 0$ for $i = 1, 2, 3$. Then, during the analysis, we fix Ψ by selecting the value of λ manually, and optimize over M .

C. Robustness analysis

Our goal is to find the radius $\rho \in \mathbb{R}^+$ of the smallest ball that covers all possible outputs at time T ($e(T)$) given that the initial states lie within an ellipsoidal set $\mathcal{E}_0 = \{\eta \in \mathbb{R}^{n_\eta} : \eta^\top A_0 \eta \leq 1, A_0 = A_0^\top \succ 0\}$ and the dynamics satisfy (19)-(20). To solve this problem, an efficient and scalable algorithm is proposed in [29, Ch. 3.1] by computing the robust \mathcal{L}_2 -to-Euclidean gain. First, a time-varying quadratic storage function is defined. Then, a dissipation inequality is formulated and integrated over the horizon. Due to the ellipsoidal set description, linear dynamics and quadratic storage function, the problem is described by *linear matrix inequalities* (LMIs) at each fixed time instant. By formulating N number of LMIs uniformly distributed over the time horizon, a semidefinite program is set up to minimize ρ .

Let ρ^* be the optimal optimal value found by the algorithm. Then, it is guaranteed that the hook will be in a ball of radius ρ^* around the reference position at the time of grasping. Hence, if the radius of the hook is larger than ρ^* , then the success of the payload grasping is ensured. In Section VI, we show that this condition is satisfied in case of realistic uncertainty and disturbance magnitudes.

VI. EXPERIMENTS

A. Experimental setup

In the experiments, we use an F1Tenth autonomous racecar [30] as a UGV with the reference tracking LPV controller introduced in [31]. To carry the 3D printed payload, a custom designed trailer is attached to the UGV. The aerial platform is also custom designed (see [13] for details), equipped with a 3D printed hook connected to a carbon fiber rod. The experimental setup is shown in Fig. 1, and the physical parameters of the manipulator are given in Table I.

For trajectory optimization, we use the following parameters: $h = 0.05$ s, $T_d = 10$, $W_R^i = 20I_4$,

$W_Q^i = \text{diag}(I_3, 0.1I_3, 0_2, 3, 0.5I_3, 0_2, I_2)$ for $i = 1, 2, 3$. The weights of the LTV-LQR controller have been set to $W_Q = W_F = \text{diag}(10I_3, I_2, 10, 0.1I_3, I_3, 0.1I_4)$, $W_R = \text{diag}(5, 40I_3)$. The numerical values of the parameters have been chosen based on preliminary simulation experiments.

B. Simulation study

To evaluate the performance of the proposed method, we use a paperclip shaped reference path for the UGV with constant speed, illustrated in Fig. 5. Different scenarios are generated by changing the speed, the time window for grasping, and the initial pose of the quadcopter.

Robustness analysis: We perform the robustness analysis with an initial ellipsoid defined by $A_0 = \text{diag}(10I_3, 100I_3, 10I_3, 100I_3, 10I_4)$, disturbance magnitude $\beta = 0.02$, and $N = 50$ discretization time steps. Moreover, as each reference trajectory results in a different LTV system, we solve the optimization by designing trajectories from 16 different initial drone positions (shown in Fig. 5, with 1.1 m initial height) and 3 UGV speed values (0.6, 0.8, 1.0 m/s), resulting in 48 optimizations altogether. Within the obtained solutions, the maximum value is $\rho^* = 0.968$ cm. The radius of the hook we use for the experiments is $r_{\text{hook}} = 2.3$ cm, which is significantly larger than ρ^* , therefore we theoretically guarantee that the grasping is accomplished despite the considered uncertainties and disturbances.

Payload grasping on rough terrain: First, we analyze the performance of the proposed method by simulating a rough terrain that is discovered continuously, motivated by the problem investigated in [32]. Each time a new part of the terrain is discovered, i) the trajectory of the UGV is simulated to update the payload motion prediction, ii) Optimization (16) is solved to update the quadcopter reference trajectory, and iii) the LQR gains are recomputed and passed to the controller. The computation time of each step significantly depends on the duration of the maneuver, because it determines the number of simulation steps and SQP shooting nodes. For a maximum of $T_f = 17$ s, the worst-case computation time of steps i)-iii) is 1.4 s on a standard laptop. Hence, new trajectories are activated 1.4 s after receiving the terrain information. By parallelizing the computations, the main simulation runs in real-time.

A specific scenario is illustrated in Fig. 6, where the upper plot shows the trajectory of the hook on the quadcopter with the path of the payload, and the lower plot shows snapshots from the MuJoCo simulation. The terrain includes 6 parts, each constructed by assigning random height values in the range of $[0, 0.12]$ m to every node on a uniform grid with 0.25 m spacing, and connecting the nodes by flat surfaces. Subsequent terrain parts appear with at least 1.4 s time difference, enabling real-time replanning of the reference trajectory. In this scenario, the mass of the payload is $m_{\text{load}} = 0.1$ kg, the reference speed of the UGV is 0.5 m/s, the time window for grasping is specified as $\underline{T}_g = 7.5$ s, $\overline{T}_g = 10.5$ s, and the duration is $T_f = 16.5$ s. The upper plot of Fig. 6 shows that the manipulator follows the payload before grasping, which naturally results from the cost definition

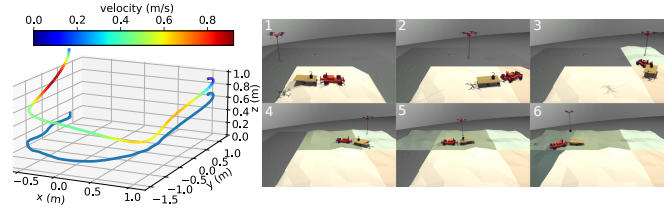


Fig. 6. Payload grasping from a moving platform on rough terrain.

of Phase 1. Then, driven by the complementarity constraints, the quadcopter accelerates to grasp the payload. Finally, the payload is transported towards the target location.

C. Real-world experiments

We evaluate the real-world performance of the proposed methods by flight experiments. Our quadcopter is equipped with a Crazyflie Bolt flight controller that runs the state estimation and LTV-LQR controller at 500 Hz. Optitrack motion capture system is used to provide high-precision pose information of the manipulator, the UGV, and the payload. The computational budget of the microcontroller is not sufficient for nonlinear optimization, therefore the trajectories are computed on a desktop PC and sent to the drone via radio. However, the real-time simulations presented before validate that a more powerful embedded computer would make it possible to run the whole algorithm onboard.

Real-world experiments begin with collecting the pose of the manipulator, the UGV, the trailer, and the payload from the motion capture system. The UGV reference tracking is forward simulated given the current position and velocity of the vehicle to obtain the payload motion prediction, and the reference trajectory of the quadcopter is designed. Fig. 1 shows photos of a grasping experiment, and the supplementary material contains videos of several scenarios².

We investigate three scenarios in detail, which are shown in Fig. 7, displaying the trajectory of the hook on the quadcopter, the position of the payload, and photos taken at the grasping time instants. These experiments have been conducted with payload mass $m_{\text{load}} = 0.1$ kg, UGV reference speed $\{0.6, 0.8, 0.8\}$ m/s, time window $\underline{T}_g = \{5.5, 4.5, 4.2\}$ s, $\overline{T}_g = \{8.5, 7.5, 7.2\}$ s, and duration $T_f = \{14.5, 13.5, 13.2\}$ s, respectively. As it is shown in the photos, the initial payload orientation has been different in each scenario. In Scenario 1, the payload forward-facing hook of the payload makes grasping more challenging than in the other configurations. However, according to (10), the designed trajectory ensures that the payload is grasped from the side, leading to a successful maneuver. In Scenario 2, the acceleration of the hook-gripper is large at Phase 1 of the trajectory, and the agile motion leads to relatively large hook angles α and β . This example shows that although the hook is not actuated, it can be controlled precisely without reducing the agility of the motion. Finally, Scenario 3 shows

²To put down the payload and land the quadcopter (shown in the supplementary video), we use the planning method of [13] with predefined waypoints, as these maneuvers are independent of the moving platform.

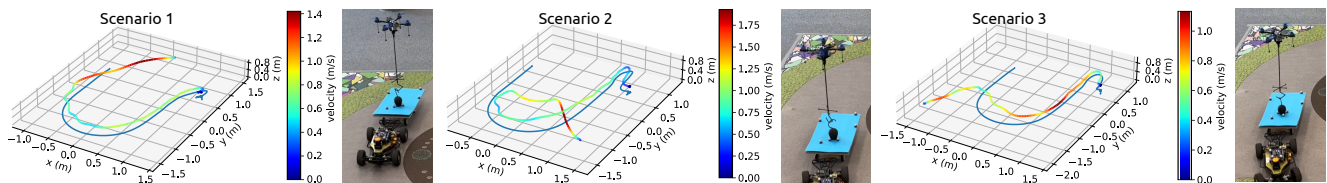


Fig. 7. Motion trajectories of the hook of the quadcopter and the payload in real flight experiments with photos of the grasping time instants.

a similar experiment with different parameters showing reliable performance of the method despite the variations of the initial conditions and specific parameter settings.

VII. CONCLUSION

In this work, we propose a complete solution for hook-based aerial payload grasping from a moving platform. The digital twin-based payload motion prediction and computationally efficient trajectory optimization enable reliable reference generation and rapid replanning in dynamically changing environments. We guarantee successful grasping under uncertainties and disturbances by IQC-based robustness analysis of the closed-loop manipulator dynamics. The experimental results show that the proposed approach is robust and efficient, enabling the hook-based manipulator to successfully grasp a small payload from a moving platform.

REFERENCES

- [1] F. Ruggiero, V. Lippiello, and A. Ollero, "Aerial manipulation: A literature review," *IEEE Robotics and Automation Letters*, vol. 3, pp. 1957–1964, 2018.
- [2] A. Ollero, M. Tognon, A. Suarez, D. Lee, and A. Franchi, "Past, present, and future of aerial robotic manipulators," *IEEE Transactions on Robotics*, vol. 38, no. 1, pp. 626–645, 2022.
- [3] G. Baraban, S. Kothiyal, and M. Kobilarov, "Perception-based UAV fruit grasping using sub-task imitation learning," in *Proc. of the Aerial Robotic Systems Physically Interacting with the Environment*, 2021, pp. 1–8.
- [4] O. Maghazei and T. Netland, "Drones in manufacturing: Exploring opportunities for research and practice," *Journal of Manufacturing Technology Management*, vol. 31, no. 1, pp. 1237–1259, 2020.
- [5] R. Spica, A. Franchi, G. Oriolo, H. H. Bulthoff, and P. R. Giordano, "Aerial grasping of a moving target with a quadrotor UAV," in *IEEE/RSJ International Conference on Intelligent Robots and Systems*, 2012, pp. 4985–4992.
- [6] G. Zhang, Y. He, B. Dai, F. Gu, L. Yang, J. Han, G. Liu, and J. Qi, "Grasp a moving target from the air: System & control of an aerial manipulator," in *IEEE International Conference on Robotics and Automation*, 2018, pp. 1681–1687.
- [7] W. Luo, J. Chen, H. Ebel, and P. Eberhard, "Time-Optimal Handover Trajectory Planning for Aerial Manipulators Based on Discrete Mechanics and Complementarity Constraints," *IEEE Transactions on Robotics*, vol. 39, no. 6, pp. 4332–4349, 2023.
- [8] H. Hua, Y. Fang, X. Zhang, and C. Qian, "A time-optimal trajectory planning strategy for an aircraft with a suspended payload via optimization and learning approaches," *IEEE Transactions on Control Systems Technology*, vol. 30, no. 6, pp. 2333–2343, 2022.
- [9] G. Li, A. Tunchez, and G. Loianno, "PCMPC: Perception-constrained model predictive control for quadrotors with suspended loads using a single camera and IMU," in *Proc. of the IEEE International Conference on Robotics and Automation*, 2021, pp. 2012–2018.
- [10] H. Li, H. Wang, C. Feng, F. Gao, B. Zhou, and S. Shen, "Auto-Trans: A Complete Planning and Control Framework for Autonomous UAV Payload Transportation," *IEEE Robotics and Automation Letters*, vol. 8, no. 10, pp. 6859–6866, 2023.
- [11] H. Wang, H. Li, B. Zhou, F. Gao, and S. Shen, "Impact-Aware Planning and Control for Aerial Robots With Suspended Payloads," *IEEE Transactions on Robotics*, vol. 40, pp. 2478–2497, 2024.
- [12] J. Thomas, G. Loianno, J. Polin, K. Sreenath, and V. Kumar, "Toward autonomous avian-inspired grasping for micro aerial vehicles," *Bioinspiration & Biomimetics*, vol. 9, no. 2, 2014.
- [13] P. Antal, T. Péni, and R. Tóth, "Autonomous hook-based grasping and transportation with quadcopters," *arXiv: 2304.02444*, 2024.
- [14] K. Sreenath, T. Lee, and V. Kumar, "Geometric control and differential flatness of a quadrotor uav with a cable-suspended load," in *Proc. of the IEEE Conference on Decision and Control*, 2013.
- [15] C. D. Crousaz, F. Farshidian, and J. Buchli, "Aggressive optimal control for agile flight with a slung load," in *Proc. of the IROS 2014 Workshop on Machine Learning in Planning and Control of Robot Motion*, 2014.
- [16] K. Sreenath, N. Michael, and V. Kumar, "Trajectory generation and control of a quadrotor with a cable-suspended load - A differentially-flat hybrid system," in *Proc. of the IEEE International Conference on Robotics and Automation*, Karlsruhe, Germany, May 2013, pp. 4888–4895.
- [17] R. W. Beard and T. W. McLain, *Small Unmanned Aircraft: Theory and Practice*. Princeton University Press, 2012.
- [18] W. T. Thomson, *Theory of Vibration with Applications*. CrC Press, 2018.
- [19] E. Todorov, T. Erez, and Y. Tassa, "Mujoco: A physics engine for model-based control," in *Proc. of the IEEE International Conference on Intelligent Robots and Systems*, 2012, pp. 5026–5033.
- [20] K. Lowrey, S. Kolev, Y. Tassa, T. Erez, and E. Todorov, "Physically-consistent sensor fusion in contact-rich behaviors," in *Proc. of the IEEE/RSJ International Conference on Intelligent Robots and Systems*, 2014, pp. 1656–1662.
- [21] H. G. Bock and K. J. Plitt, "A Multiple Shooting Algorithm for Direct Solution of Optimal Control Problems," in *Proc. of the 9th IFAC World Congress: A Bridge Between Control Science and Technology*, 1984, pp. 1603–1608.
- [22] R. Verschuere, G. Frison, D. Kouzoupis, J. Frey, N. V. Duijkeren, A. Zanelli, B. Novoselnik, T. Albin, R. Quirynen, and M. Diehl, "acados—a modular open-source framework for fast embedded optimal control," *Mathematical Programming Computation*, vol. 14, no. 1, pp. 147–183, 2022.
- [23] W. B. Greer and C. Sultan, "Shrinking Horizon Model Predictive Control Method for Helicopter–Ship Touchdown," *Journal of Guidance, Control, and Dynamics*, vol. 43, no. 5, pp. 884–900, 2020.
- [24] H. Kwakernaak and R. Sivan, *Linear optimal control systems*. New York: Wiley Interscience, 1972.
- [25] G. Torrente, E. Kaufmann, P. Fohn, and D. Scaramuzza, "Data-Driven MPC for Quadrotors," *IEEE Robotics and Automation Letters*, vol. 6, no. 2, pp. 3769–3776, 2021.
- [26] P. Seiler, R. M. Moore, C. Meissen, M. Arcak, and A. Packard, "Finite horizon robustness analysis of LTV systems using integral quadratic constraints," *Automatica*, vol. 100, pp. 135–143, 2019.
- [27] A. Megretski and A. Rantzer, "System analysis via integral quadratic constraints," *IEEE Transactions on Automatic Control*, vol. 42, no. 6, pp. 819–830, 1997.
- [28] J. Veenman, C. W. Scherer, and H. Köroğlu, "Robust stability and performance analysis based on integral quadratic constraints," *European Journal of Control*, vol. 31, pp. 1–32, 2016.
- [29] R. M. Moore, "Finite horizon robustness analysis using integral quadratic constraints," Master's thesis, University of California, Berkeley, 2015.
- [30] M. O'Kelly, H. Zheng, D. Karthik, and R. Mangharam, "Fltenth: An open-source evaluation environment for continuous control and reinforcement learning," in *Proc. of the NeurIPS Competition and Demonstration Track*, vol. 123, 2019, pp. 77–89.
- [31] K. Floch, T. Péni, and R. Tóth, "Gaussian-process-based adaptive trajectory tracking control for autonomous ground vehicles," in *Proc. of the European Control Conference*, 2024, pp. 464–471.

- [32] N. Aoki and G. Ishigami, "Hardware-in-the-loop Simulation for Real-time Autonomous Tracking and Landing of an Unmanned Aerial Vehicle," in *Proc. of the IEEE/SICE International Symposium on System Integration*, 2023, pp. 1–6.